Ionics (2014) 20:1747–1755
DOI 10.1007/s11581-014-1137-9

ORIGINAL PAPER

The influence of sodium gluconate on nickel and manganese codeposition from acidic chloride-sulfate baths

Ewa Rudnik · Grzegorz Włoch

Received: 11 February 2014 / Revised: 1 April 2014 / Accepted: 18 April 2014 / Published online: 9 May 2014

Abstract Nickel and manganese were codeposited from acidic chloride-sulfate solution in the presence and without sodium gluconate as complexing and buffering agent. Equilibrium pH-dependent distribution of soluble species in the baths was calculated. Deposition of metals was studied by cyclic voltammetry and Hull cell tests. Deposits were obtained in potentiostatic (−1.6 to −1.7 V vs. Ag/AgCl) and galvanostatic (4–8 A/dm^2) conditions. It was found that the buffering action of gluconate ions improved the quality of the deposits, and compact Ni-Mn with a grid of fine crack layers was produced. The additive inhibited the formation of nonmetallic inclusions represented by decreased oxygen content in the deposits. Layers produced at constant potentials contained 67–79 % Ni, 1–8 % Mn, and 15–30 % O. Under galvanostatic conditions, the average compositions were in the range of 18–80 % Ni, 2–48 % Mn, and 17–42 % O. Despite of the bath composition, the main cathodic reaction was hydrogen evolution resulting in very low amounts of the cathodic deposits.

Keywords Manganese · Nickel · Electrolysis · Gluconate

Introduction

Over the last decade, some interest in electrodeposited manganese-nickel coatings has been observed. It is mainly due to their magnetic properties and potential usefulness for microsystem applications [1–9]. A first review of the papers and patents concerning the possibility of manganese and nickel codeposition was presented in the monograph of Brenner in the 1960s [10]. Later, a relatively small number of studies in this field has been published.

Electrodeposition of manganese and its alloys with nickel or other metals (e.g., Co, Sn, etc.) using simple salt aqueous solutions is relatively difficult. This is primarily due to the very low value of the Mn/Mn^{2+} equilibrium electrode potential ($E°_{Mn/Mn2+}$=−1.18 V vs. NHE), while the potential of the Ni/Ni^{2+} electrode is much higher ($E°_{Ni/Ni2+}$=−0.25 V vs. NHE). It suggests that nickel can deposit preferentially in comparison to manganese. However, considering codeposition of two or more metals solely according to the values of the standard (or equilibrium) electrode potentials is erroneous. Deposition overvoltages of the individual metals should be also taken into account, since they are significantly dependent on the electrolysis conditions (composition of the bath, current density/cathode potential, temperature, etc.). Additional complication during Ni-Mn codeposition can arise from the selection of the electrolyte pH. Electrodeposition of manganese should be carried out in the solutions of pH above 2 to prevent intensive hydrogen coevolution, but in a more alkaline environment, hydrolysis and precipitation of various manganese hydroxides/oxides can occur [11]. In the case of nickel, the best conditions for the electrodeposition are achieved in the baths with pH of approx. 4 [12].

Ni-Mn alloys were usually obtained from sulfamate baths with the addition of chloride ions, at pH 3.5–4.0 [1–7, 9]. The solutions contained more than 1 M Ni^{2+}, while the Mn^{2+} concentration was only 0.009–0.09 M. Films were produced in galvanostatic [1–5, 9] or pulse current [1, 2] modes using current densities from the range of 0.1–4 A/dm^2. Under these conditions and at room temperature, the alloys contained less than 1.2 wt% Mn and the composition of the deposits corresponded to the concentration ratios of the metals in the solutions. Simultaneously, a strong dependence of the manganese content in the alloys on the current density was found, whereas no effect of the current type (direct or pulse) was observed.

E. Rudnik (✉) · G. Włoch
Faculty of Non-Ferrous Metals, AGH University of Science and Technology, Al. Mickiewicza 30, 30-059 Cracow, Poland
e-mail: erudnik@agh.edu.pl

Table 1 Composition of the baths

Component	Ni	Ni-Glu	Mn	Mn-Glu	Ni-Mn	Ni-Mn-Glu
	Concentration, M					
$MnSO_4$	–	–	0.5	0.5	0.5	0.5
$NiSO_4$	0.1	0.1	–	–	0.1	0.1
NH_4Cl	0.5	0.5	0.5	0.5	0.5	0.5
H_3BO_3	0.5	0.5	0.5	0.5	0.5	0.5
Na-Glu	–	0.2	–	0.2	–	0.2

Stephen et al. [6, 7] obtained Ni-Mn alloys from acidic sulfate baths (pH 3) of various Mn^{2+}/Ni^{2+} concentration ratios, at room temperature, and at the current density of 3 A/dm^2. Cathodic deposits contained 71–97 wt% Ni. The authors also determined the magnetic properties of the materials. They found that the Ni-Mn deposits showed higher magnetic coercivity than pure nickel, but the increase in the nickel content resulted in a further beneficial effect on the magnetic properties of the alloys.

Chloride solutions of pH 6.5 were used by Fathi and Sanjabi [8]. The authors reported that at the Mn^{2+}/Ni^{2+} concentration ratio equaled 1, less than 1 wt% of manganese was present in the deposits, while for the Mn^{2+}/Ni^{2+} concentration ratio 2.5 manganese content in the alloys was in the range of 2–9 wt%, depending on the applied current density.

There is no information in the literature on the codeposition of the Ni-Mn alloys from complex salt solutions. A proper selection of the concentration ratio of the metal ions to ligand should close the potentials of nickel and manganese electrodes due to a decrease in the concentration of free metal ions in the electrolyte as a result of a complex formation. Hence, the aim of this work was to determine the influence of sodium gluconate addition as Ni^{2+} complexing agent [13] on the codeposition of metals from acidic chloride-sulfate baths. Such additive was used successfully for electrodeposition of manganese alloys with tin [14] or cobalt [15], while to date, no attempts for nickel-manganese codeposition have been reported.

Experimental

Electrodeposition was carried out from solutions with the compositions presented in Table 1. Sodium gluconate (Na-Glu) was used as both complexing and buffering agent [13]. The pH of all baths was 3.5. Blank solutions of similar compositions were prepared using 0.1 M $(NH_4)_2SO_4$ instead of nickel and manganese salts. Reagents of analytical purity were used.

Equilibrium distributions of the species for the baths used in this study were calculated using "HySS 2008" free software for stability complex constants adopted from adequate references.

Electrochemical measurements were carried out in a three-electrode cell using glassy carbon (0.2 cm^2) or α-brass (10 wt% Zn; 0.8 cm^2) as working electrodes, a platinum plate (2 cm^2) as a counter electrode, and an Ag/AgCl as reference electrode. All potentials in the succeeding text referred to this electrode. Before each experiment, the glassy carbon electrode with a mirror finish was chemically cleaned, while brass sheets were chemically polished in a mixture of concentrated acids ($HNO_3/H_3PO_4/CH_3COOH$ with 1:3:1 volume ratio).

Cyclic voltammograms were registered using the GC electrode at a potential scan rate of 20 mV/s with a first sweep performed from the initial potential toward more negative values. A solution volume of 25 cm^3 was used in each electrochemical experiment. The Hull cell was used to determine the range of the cathodic current densities for galvanostatic deposition. Measurements were performed at the current intensity of 1.5 A for 10 min using 0.2 dm^3 of the bath, copper

Table 2 Equilibrium constants at 298 K [19, 20]

Reaction	Equilibrium quotient	Constant
$Mn^{2+} + H_2O \leftrightarrow MnOH^+ + H^+$	$\beta_1 = \frac{[MnOH^+][H^+]}{[Mn^{2+}]}$	$\log \beta_1 = -10.59$
$Mn^{2+} + 2H_2O \leftrightarrow Mn(OH)_{2\ aq} + 2H^+$	$\beta_2 = \frac{[Mn(OH)_2][H^+]^2}{[Mn^{2+}]}$	$\log \beta_2 = -22.42$
$Mn^{2+} + 3H_2O \leftrightarrow Mn(OH)_3^- + 3H^+$	$\beta_3 = \frac{[Mn(OH)_3^-][H^+]^3}{[Mn^{2+}]}$	$\log \beta_3 = -34.81$
$Mn^{2+} + Cl^- \leftrightarrow MnCl^+$	$\beta_1 = \frac{[MnCl^+]}{[Mn^{2+}][Cl^-]}$	$\log \beta_1 = 0.607$
$Mn^{2+} + 2Cl^- \leftrightarrow MnCl_2$	$\beta_2 = \frac{[MnCl_2]}{[Mn^{2+}][Cl^-]^2}$	$\log \beta_2 = 0.041$
$Mn^{2+} + 3Cl^- \leftrightarrow MnCl_3^-$	$\beta_3 = \frac{[MnCl_3^-]}{[Mn^{2+}][Cl^-]^3}$	$\log \beta_3 = -0.305$
$Mn^{2+} + SO_4^{2-} \leftrightarrow MnSO_4$	$\beta_1 = \frac{[MnSO_4]}{[Mn^{2+}][SO_4^{2-}]}$	$\log \beta_1 = 2.25$
$Mn^{2+} + 2SO_4^{2-} \leftrightarrow Mn(SO_4)_2^{2-}$	$\beta_2 = \frac{[Mn(SO_4)_2^{2-}]}{[Mn^{2+}][SO_4^{2-}]^2}$	$\log \beta_2 = 1.87$
$Mn^{2+} + 2HGlu^- \leftrightarrow MnGlu_2 + 2H^+$	$K = \frac{[MnGlu_2][H^+]^2}{[Mn^{2+}][HGlu]^2}$	$\log K = -16.48$

cathode, and platinum anode. Potentiostatic or galvanostatic deposition was carried out with brass plates as cathode substrates and 25 cm^3 of the electrolyte. All measurements were carried out without any agitation of the solutions. Autolab potentiostat/galvanostat (PGSTAT30) controlled by a microcomputer was used.

The morphology of the layers was examined using a scanning electron microscope (Hitachi). The chemical composition of the deposits was determined by means of EDS-SEM, and the presented results are average values of the analyses performed on five areas (per sample) on the deposits' surface. The structure of the layers was analyzed by X-ray diffractometry.

Buffer actions of the blank and 0.2 M sodium gluconate solutions were determined by slow addition (Crison titrator) of 0.1 M HCl or 0.1 M NaOH to 20 cm^3 of the electrolyte until pH was changed from 3.5 to a final value of 2.5 or 4.5, respectively. All measurements were performed at the temperature of 21±1 °C.

Results and discussion

Distribution of Ni(II) and Mn(II) species

Usually, nickel or manganese is deposited using chloride, sulfate, or mixed acidic baths [9, 12, 13, 16–18]. Electrodeposition of manganese is carried out from both chloride- and sulfate-based electrolytes containing corresponding ammonium salts [16–18]. Ammonium salts, mainly sulfate, suppress the precipitation of manganese hydroxides, improve the conductivity of the solutions, provide a desirable buffering effect at pH 2–3.5, and increase the ability of the manganese ion discharge [18]. Earlier research on the nickel electrodeposition from acidic baths containing ammonium salts [13] demonstrated that the chloride solution shows better properties than the sulfate one due to higher salt solubility and higher cathodic current efficiencies achieved. A chloride-sulfate bath allowed obtaining deposits with the thickness and cathodic current efficiencies similar to those observed in the chloride bath, but at improved buffer capacity of the electrolyte.

In the present study, a chloride-sulfate bath was adopted for nickel and manganese codeposition. Since nickel is the nobler metal in the system, the Ni^{2+}/Mn^{2+} concentration ratio in the bath was 0.2 to shift the nickel electrode potential toward

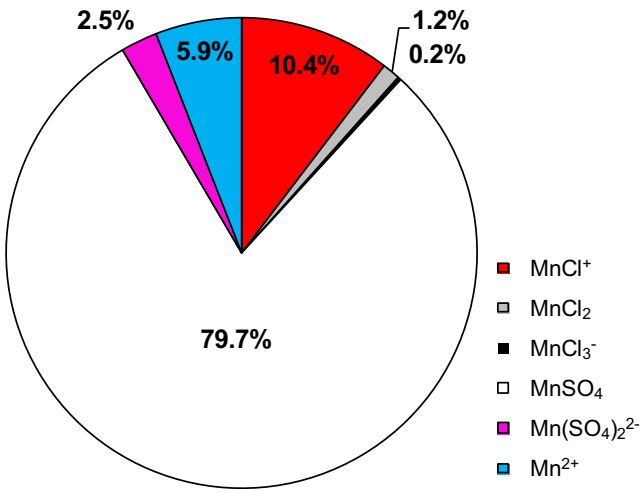

Fig. 1 Distribution of main Mn(II) species in the chloride-sulfate baths used in this study (at pH 3.5)

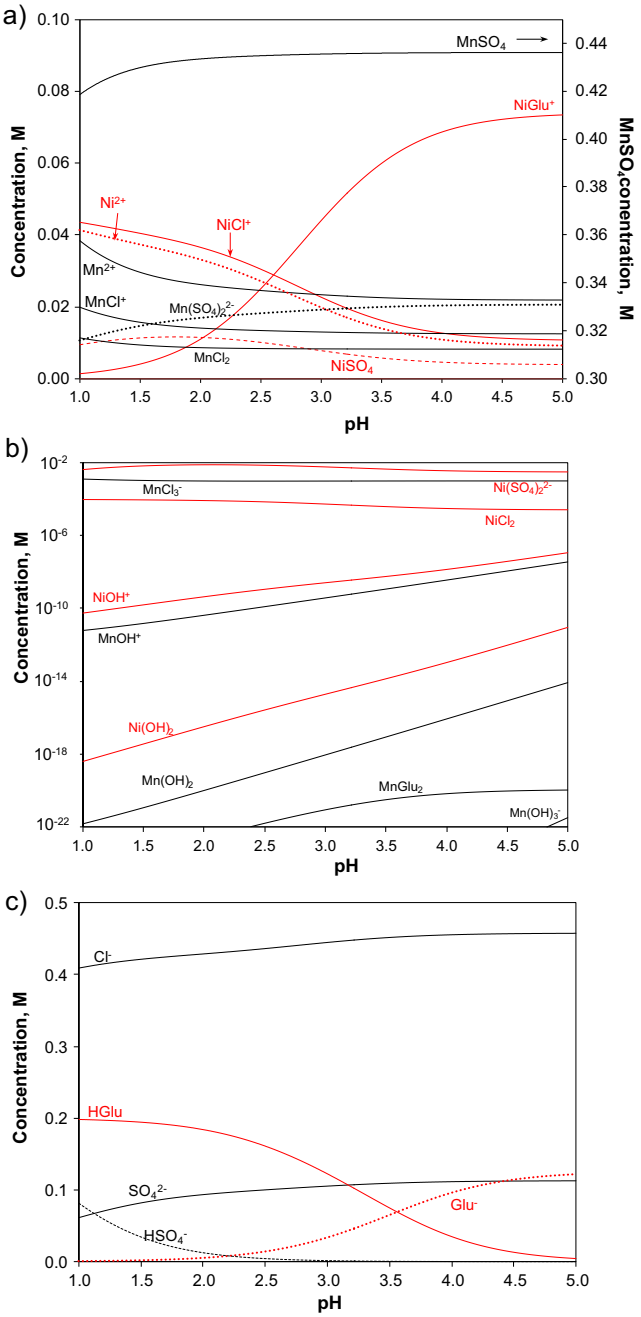

Fig. 2 **a**–**c** pH-dependent equilibrium distribution of species in the Ni-Mn-gluconate bath (with composition presented in Table 1)

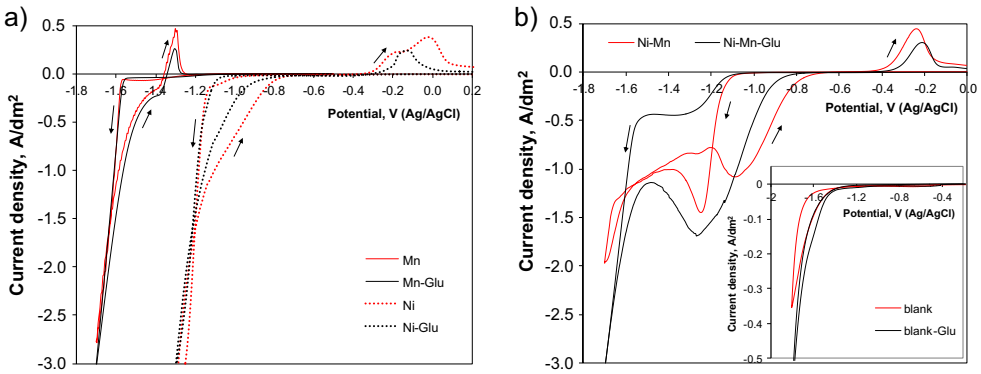

Fig. 3 Cyclic voltammograms registered in **a** single salt solutions and **b** nickel-manganese baths

more negative values. In the presence of sodium gluconate, two additional phenomena were expected: the sole formation of nickel-gluconate complexes and an increase in the buffer capacity of the solutions, which is the most important factor responsible for maintaining stable pH during electrolysis.

To verify the above assumptions, speciation of the electrolytes was determined. The concentrations of the individual species were calculated from the equilibrium quotients assigned to the reactions presented in Table 2 for manganese ions and elsewhere [13] for nickel ions.

Previous studies [13] have shown that nickel-gluconate complexes can be formed in the acidic solutions, and the $Ni\text{-}Glu^{+}$ complex represents 67 % of the nickel species in the chloride-sulfate bath at pH of 3.5. Literature data shows that gluconate can form stable complexes with Mn^{2+} cations only in strongly alkaline solutions [11, 20, 21]. Escandar et al. [22] reported that in the acid region, the possible Mn(II)-gluconate complexes formed were not stable enough to be potentiometrically detected, while at pH above 7, precipitation of manganese hydroxide was observed. Equilibrium distribution of manganese species calculated for two manganese baths used in this study confirmed that the presence of sodium gluconate practically does not change the speciation of the solution and

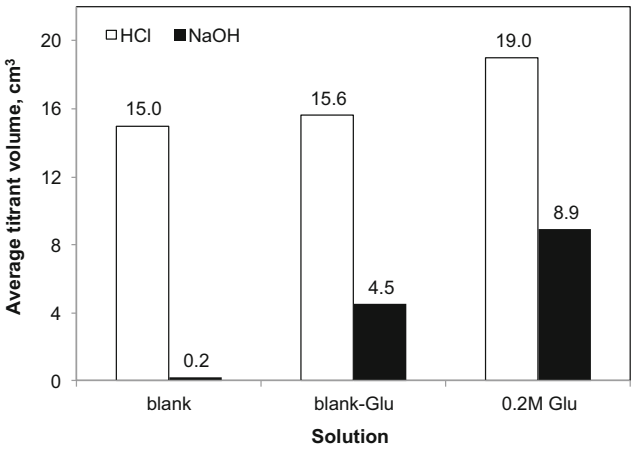

Fig. 4 Volume of 0.1 M HCl or 0.1 M NaOH necessary to change the pH of blank solutions and 0.2 M sodium gluconate solution from 3.5 to 2.5 or 4.5, respectively

$MnSO_4$ is the dominating complex in both electrolytes (Fig. 1).

Figure 2 shows speciation of the nickel-manganese solution in the presence of gluconate ions. As it was expected, $MnSO_4$ and $Ni\text{-}Glu^{+}$ remain the most stable and main species in the solution of pH 3.5 and represent 87 and 60 % of the total manganese and nickel ions concentrations, respectively. Free Ni^{2+} and $NiCl^{+}$ ions show comparable percentages in the bath (14 and 16 %, respectively). Other chloride or hydroxide complexes appear in much less fractions.

Equilibrium speciation does not predict precipitation of metal hydroxides in the pH range considered despite of low solubility products of both hydroxides ($pL_{Ni(OH)2}=11.9$; $pL_{Mn(OH)2}=12.9$). This is consistent with the *E*-pH diagrams for both metal-H_2O systems, where precipitation of $Ni(OH)_2$ and $Mn(OH)_2$ is expected at pH above 7 [23].

Potentiostatic deposition

Cathodic potentials for the metal deposition were selected according to the data obtained in the cyclic voltammetric measurements. Figure 3 shows the CV curves registered in the nickel, manganese, and nickel-manganese solutions on the glassy carbon substrate. It is known that overvoltage of hydrogen evolution on the glassy carbon is high; hence, it makes possible to "separate" some essential electrode reactions (i.e., metal deposition) from hydrogen evolution at low cathode potentials.

Table 3 Current efficiency of potentiostatic manganese deposition (30 min)

Bath	Potential, V (Ag/AgCl)	Mass of deposit, mg/cm^2	Charge, C	Current efficiency, %
Mn	−1.60	0.6	14.38	12.2
	−1.65	0.5	18.71	7.5
	−1.70	0.3	22.82	3.1
Mn-Glu	−1.60	3.1	23.91	36.7
	−1.65	0.2	32.27	0.9
	−1.70	0.3	21.57	3.3

Table 4 Average composition of potentiostatically deposited Ni-Mn layers (30 min)

Bath	Potential, V (Ag/AgCl)	Charge, C	Mass of deposit, mg/cm^2	Composition, wt%		
				Ni	Mn	O
Ni-Mn	−1.60	33.45	0.4	74.3±4.8	1.0±0.2	24.7±4.9
	−1.65	37.49	0.5	67.5±7.9	2.9±0.9	29.5±17.0
	−1.70	39.76	0.8	72.5±0.2	3.2±0.9	24.3±0.8
Ni-Mn-Glu	−1.60	54.99	1.3	78.5±0.7	5.4±0.6	16.0±0.8
	−1.65	55.68	1.4	79.3±1.0	5.8±1.1	14.9±0.4
	−1.70	60.68	1.4	71.7±1.5	7.6±0.5	20.7±1.3

Nickel and manganese are metals with a high difference of deposition potentials (Fig. 3a). Electroreduction of Ni^{2+} ions starts below −1.1 V (vs. Ag/AgCl), whereas the cathodic currents for manganese were observed at approx. −1.6 V. Comparison of the initial deposition potentials with the equilibrium potentials for both metal electrodes shows that deposition of nickel is accompanied by high overvoltage ($E_{o,Ni/Ni2+}$=−0.5 V for 0.1 M Ni^{2+} vs. Ag/AgCl), while manganese ions can be reduced at the potentials closed to the equilibrium potential value ($E_{o,Mn/Mn2+}$=−1.4 V for 0.5 M Mn^{2+} vs. Ag/AgCl). However, the latter process is seriously interrupted by the hydrogen coevolution occurring below −1.5 V on the glassy carbon substrate (inset in Fig. 3b). It was confirmed in other voltammetric measurements realized on the copper substrate, where hydrogen evolved below −1.2 V. This leads to the inhibition of the metallic manganese deposition, and no anodic peak corresponding to the manganese dissolution was observed in the backward scan (results not shown).

It is worth to note that the electrodeposition of any metal on the glassy carbon surface is generally hindered. This nucleation barrier reveals in all cyclic voltammograms as lower cathodic currents recorded in the forward sweep than during the reverse step. It is obvious, since the energy required for the metal overpotential deposition on the foreign substrate is higher than that for the metal deposition on the native layer formed during the previous scan. Taking this into account, the stop of metal deposition in the positive-going part of the CV curves might be also considered as a criterion for the potential regime of metal deposition. In such case, more positive potentials (below −0.8 and −1.3 V for nickel and manganese, respectively) for the metal electrodeposition can be found.

The addition of sodium gluconate to the baths does not change deposition potentials, but it influences the "efficiency" of the metal deposition represented by the anodic responses on the CV curves. For both single metal salt systems, some inhibition of the cathodic process may be expected. It seems that for manganese bath, this results mainly from the buffering action of the gluconate species. Earlier studies on the manganese deposition [17] have shown that during the potential scan toward the negative direction, formation of $Mn(OH)_2$ was observed due to an increase in pH in the vicinity of the working electrode caused by hydrogen evolution. At more negative potentials (below −1.7 V vs. Ag/AgCl), formation of manganese and inclusion of hydroxide in the deposit were reported. In the presence of gluconate, pH changes of the chloride-sulfate solution are harder to achieve (Fig. 4), since free gluconate ions can transform into undissociated molecules of weak gluconic acid under strong acid addition or a reverse process occurs when a strong base is added (Fig. 2c). Therefore, precipitation of hydroxide may be hindered resulting in a less amount of deposited layer.

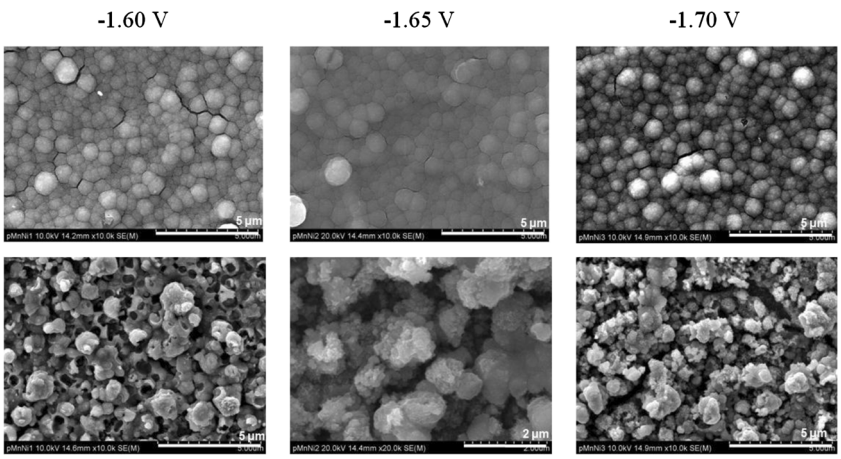

Fig. 5 Surface morphology of the cathodic deposits obtained potentiostatically from Ni-Mn bath: at the middle (*top*) and at the edges (*bottom*) of the cathode

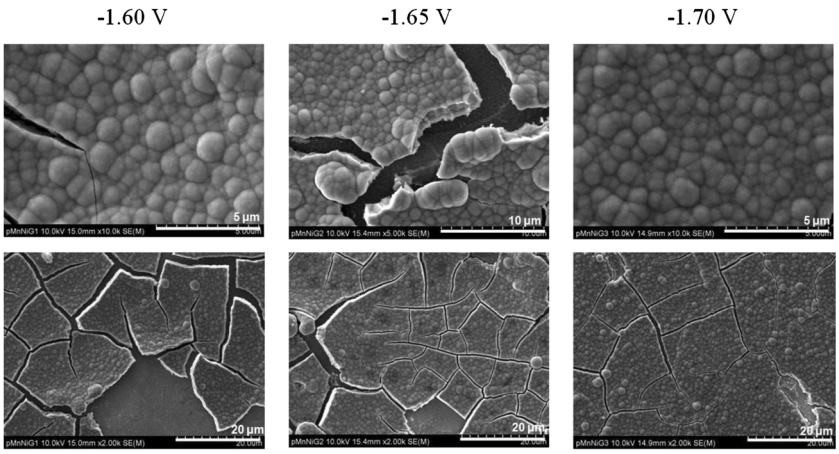

Fig. 6 Surface morphology of the cathodic deposits obtained potentiostatically from Ni-Mn-Glu bath

A similar phenomenon can occur in the nickel solutions, where an anodic peak with two shoulders (at −0.17 and 0 V) was observed in the absence of sodium gluconate. This could be attributed to the dissolution of two nickel-hydrogen alloys [13]. Fleischmann and Saraby-Reintjes [24] showed that two types of nickel deposits can be produced in the Watts type bath (pH 3.5): α-Ni—a solid solution of H in Ni, dissolving at approx. −0.08 V (vs. Ag/AgCl); and β-Ni—an interstitial hydrogen alloy of nickel dissolving at approx. −0.18 V (vs. Ag/AgCl). The addition of gluconate ions slightly inhibited the deposition of nickel from Ni-Glu^{+} complexes, but incorporation of hydrogen atoms was delayed due to the buffering action of the bath. Speciation of the bath showed that even though gluconate ion concentration was only 40 % of the total nickel ions concentration, it was enough to the effective decrease of the free Ni^{2+} amount in the solution (Fig. 2). However, the initial potentials of nickel deposition remained practically the same, independent of the presence of gluconate. Therefore, it is accepted that Ni-Glu^{+} complexes can play rather a role of "the reservoir" for free nickel ions consumed directly in the cathodic reaction.

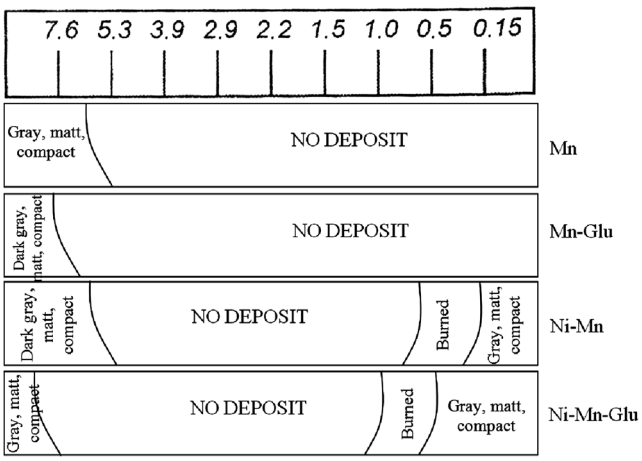

Fig. 7 Distribution of metal deposits on the cathode in the Hull cell (the current density scale in A/dm^2)

The simultaneous presence of nickel and manganese salts totally changes the course of the CV curves (Fig. 3b). During the forward scan, distinct cathodic peak corresponding to the nickel deposition was developed at the potential of approx. −1.2 V, but at more negative values, a sudden increase in the currents was observed due to the parallel run of manganese and hydrogen ion reduction. With the sodium gluconate addition, reduction of nickel ions was hindered as evidenced by the plateau on the curve in the potential range from approx. −1.3 to about −1.6 V. It shows that the codeposition of metals can affect each other as well as the reduction of hydrogen ions. The electrodeposition of nickel on the GC substrate catalyzes hydrogen evolution, while manganese suppresses the reduction of hydrogen ions. It is not excluded that firstly the deposited nickel grains make conditions suitable for favorable manganese electrodeposition or adsorption of some manganese species (e.g., produced in the secondary reactions due to some pH increase at the cathode surface), which further inhibit somewhat the hydrogen coevolution on the electrode. In the backward scan, only one anodic peak at the potential of −0.25 V was found, while no anodic oxidation of manganese was detected. It is worth to note that anodic responses in both Ni-Mn systems are shifted toward more negative values in

Table 5 Current efficiency of galvanostatic deposition (60 min)

Bath	Current density, A/dm^2	Mass of deposit, mg/cm^2	Current efficiency, %
Mn	4.0	14.1	35.1
	6.0	9.4	15.3
	8.0	6.9	8.4
Mn-Glu	4.0	11.3	27.6
	6.0	4.8	7.8
	8.0	2.8	3.4
Ni	4.0	10.1	24.8
Ni-Glu	4.0	14.3	35.0

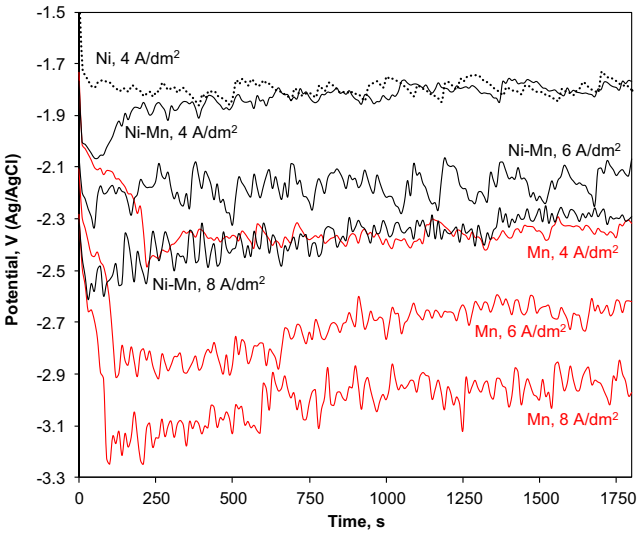

Fig. 8 Chronopotentiometric curves registered during galvanostatic deposition of metals from gluconate baths

comparison with the nickel ones, indicating a change in the composition of the deposited layer.

Potentiostatic deposition of manganese alone or with nickel was performed at the potentials from the narrow range of −1.6 to −1.7 V. Data summarized in Table 3 show that reduction of Mn^{2+} ions is very difficult as evidenced by the very low current efficiencies (cathodic current efficiency was calculated based on the mass gain of the cathode and the charge flowing through the circuit during electrolysis). The presence of sodium gluconate increased the cathodic efficiency only for −1.6 V. At lower potentials, reduction of hydrogen ions was the dominant electrode reaction, especially in the gluconate bath, where higher charges were flowed through the working electrode.

Electrodeposition in the Ni-Mn systems resulted again in very small quantities of the cathodic deposits (Table 4) because the main cathode reaction remained hydrogen evolution. Deposits contained both nickel and manganese, but also significant amounts of oxygen. The latter is often detected in the electrodeposited manganese or manganese alloys [15, 18] as a consequence of local pH change out of the buffering range of the bath. The addition of sodium gluconate increased over twice the manganese contents in the layers and seriously decreased oxygen percentage, while the fraction of nickel was relatively the same. This confirms that the buffering action of sodium gluconate prevents in some degree the precipitation of $Mn(OH)_2$ in a secondary reaction.

Figure 5 shows the surface morphology of the Ni-Mn deposits obtained in the electrolyte without sodium gluconate. Thin films were dense with a nodular structure similar to that for pure nickel [13]. However, at the edges of the cathode, where hydrogen was intensively evolved, very porous deposits with nonmetallic inclusions were formed. In these areas, some amounts of oxygen, sulfur, and chlorine were detected indicating the secondary processes at the cathode surface.

Figure 6 shows the surface of the coatings deposited in the presence of sodium gluconate. Thin layers were uniform and composed of semispherical structures. However, the whole surface of the deposits characterized with a grid of fine cracks was caused by increased internal stresses in the deposits.

Due to the small thickness of the deposits, phase analysis did not reveal any expected results, and the peaks characteristic for the brass substrate were registered. Similar negative results were obtained for low-angle X-ray diffraction analysis.

Galvanostatic deposition

Conditions for the galvanostatic deposition of metals were determined in the Hull cell. Figure 7 shows the schematic distribution of the deposits on the cathode depending on the current density. Manganese deposited only at high current densities (above 5 A/dm^2), while nickel was obtained at much lower current densities. These findings arose from the significant differences in both the reduction potentials of the metals and the salt concentrations in the baths. The results of the measurements carried out in the Hull cell are only estimated; therefore, further deposition was carried out in a wider range of the current density (4–8 A/dm^2).

Table 5 summarizes the data obtained during the manganese deposition in the galvanostatic conditions. Considerable current efficiencies were obtained for 4 A/dm^2, but at higher current densities, cathode efficiency gradually decreased.

Table 6 Composition of galvanostatically deposited Ni-Mn layers (30 min)

Bath	Current density, A/dm^2	Mass of deposit, mg/cm^2	Composition, wt%		
			Ni	Mn	O
Ni-Mn	4.0	1.8	19.5±1.7	41.9±2.2	38.6±2.7
	6.0	0.9	18.3±4.8	48.3±2.7	33.4±6.5
Ni-Mn-Glu	4.0	0.5	80.5±1.0	2.6±0.4	16.9±0.7
	6.0	8.9	76.0±0.7	2.7±0.3	21.3±0.4
	8.0	2.5	43.8±15.5	13.8±6.2	42.4±11.1

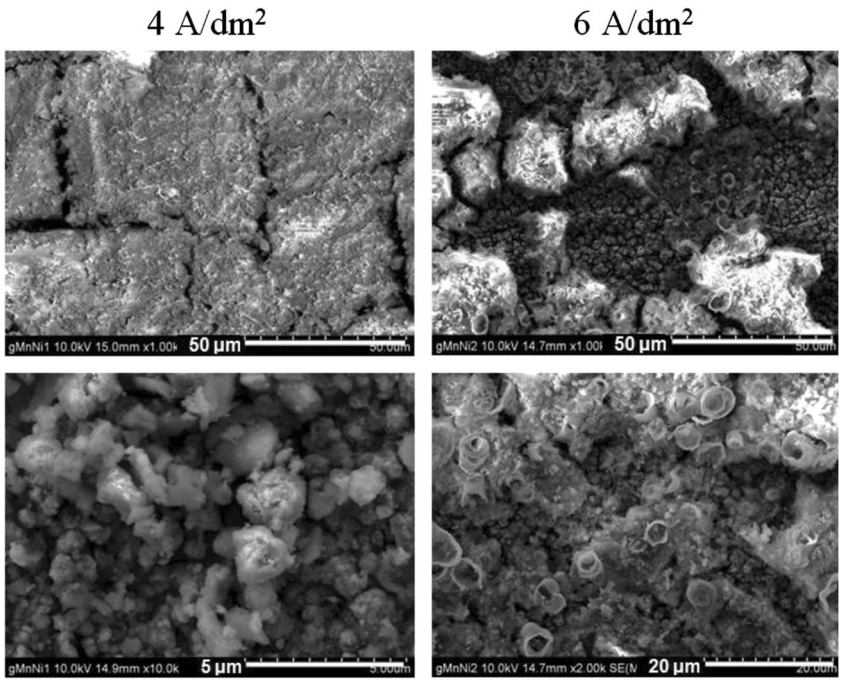

Fig. 9 Surface morphology of the cathodic deposits obtained from Ni-Mn bath in galvanostatic conditions

Applied current densities corresponded to much more negative deposition potentials in comparison to the potentiostatic conditions. Figure 8 shows chronopotentiometric curves registered in the gluconate baths. Despite that initial manganese deposition potentials were approx. −1.7 V, they decreased due to the formation of new phases at potentials below −2 V. As the current pulse was applied, there was an initial very sharp decrease in the potential caused by the charging of the double layer, but then the value at which reduction occurred on the cathode was reached. The jump of the electrode potential caused by the depletion of the solution at the electrode surface with the electroactive ions is associated with a "transition time," which was relatively long in the manganese solution and reached 100–220 s. It was mainly due to the fact that two types of the cations took part in the cathodic reactions, with dominating hydrogen evolution corresponding to the irregular course of the curves.

Table 6 shows the results obtained during manganese codeposition with nickel. At high current densities, reduction of hydrogen ions dominated resulting in the secondary products in the deposits represented by the increased oxygen content. It is not excluded that deposition of manganese can

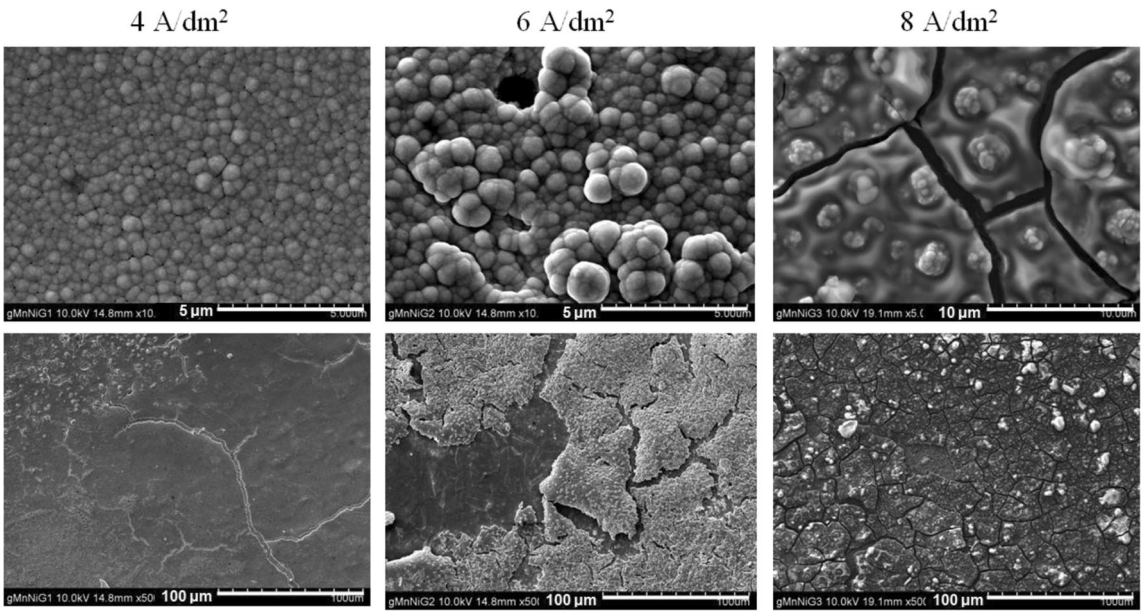

Fig. 10 Surface morphology of the cathodic deposits obtained from Ni-Mn-Glu bath in galvanostatic conditions

occur not only by the direct reduction of manganese ions, but also via $Mn(OH)_2$ formation as an intermediate product:

$$Mn(OH)_2 + 2e \rightarrow Mn + 2\ OH^- \quad (1)$$

especially that the standard potential of this redox system is −1.78 V (vs. Ag/AgCl) [23]. A similar mechanism can apply to nickel ion reduction at very negative potentials, when intensive hydrogen evolution alkalizes the solution at the cathode surface:

$$Ni(OH)_2 + 2e \rightarrow Ni + 2\ OH^- \quad E^\circ = -0.94\ V\ (vs.Ag\ \ AgCl) \quad (2)$$

Sodium gluconate significantly facilitated the deposition of nickel in the Ni-Mn system. It is consistent with the chronopotentiometric data (Fig. 8), which show that codeposition of metals runs at higher potentials than pure manganese.

Figures 9 and 10 show the morphologies of the cathode deposits. In the absence of sodium gluconate, thin and loose layers were deposited, composed mainly of numerous nonmetallic inclusions. At the areas of the most intensive hydrogen evolution characteristic, tube structures were formed. Sodium gluconate improved the quality of the deposits. These were compact films with a grid of cracks changing gradually into deposits with nonmetallic inclusions at higher current densities. Compact areas were composed of spherical metallic grains.

Conclusions

Codeposition of nickel and manganese was carried out in the acidic chloride-sulfate solution in the presence and without sodium gluconate as the complexing and buffering agent. Due to the significant difference in electrochemical potentials of manganese and nickel electrodes and a very low value of the manganese electrode potential, the dominant cathodic reaction was hydrogen evolution. This resulted in the alkalization of the electrolyte at the cathode surface and hydrolytic precipitation of inorganic compounds. It produced cathode deposits as a mixture of metallic phases and nonmetallic inclusions. The presence of sodium gluconate improved the quality of the deposits and decreased oxygen content in the cathodic deposits.

Acknowledgments This research work was realized under Project No. AGH 11.11.180.373.

References

1. Atanassov N, Mitreva V (1996) Electrodeposition and properties of nickel-manganese layers. Surf Coat Technol 78:144–149
2. Kelly JJ, Goods SH, Yang NYC (2003) High performance nanostructured Ni-Mn alloy for microsystem applications. Electrochem Solid State Lett 6(6):C88–C91
3. Goods SH, Kelly JJ, Yang NYC (2004) Electrodeposited nickel-manganese: an alloy for microsystem applications. Microsyst Technol 10:498–505
4. Yang NYC, Headley TJ, Kelly JJ, Hruby JM (2004) Metallurgy of high strength Ni-Mn microsystems fabricated by electrodeposition. Scri Mater 51:761–766
5. Talin AA, Marquis EA, Goods SH, Kelly JJ, Miller MK (2006) Thermal stability of Ni-Mn electrodeposits. Acta Mater 54:1935–1947
6. Stephen A, Nagarajan T, Ananth MV (1998) Magnetization behaviour of electrodeposited Ni-Mn alloys. Mater Sci Eng B55:184–186
7. Stephen A, Ananth MV, Ravichandran V, Narashiman BRV (2000) Magnetic properties of electrodeposited nickel-manganese alloys: effect of Ni/Mn bath ratio. J Appl Electrochem 30:1313–1316
8. Fathi R, Sanjabi S (2012) Electrodeposition of nanostructured $Ni_{(1-x)}Mn_x$ alloys films from chloride bath. Curr Appl Phys 12:89–92
9. Zhu Z, Li X, Zhu D (2013) Mechanical electrodeposition of Ni-Mn alloy. Mater Manuf Proc 28(12):1301–1304
10. Brenner A (1963) Electrodeposition of alloys. Academic Press, NY
11. Wekesa M, Uddin J, Sobhi HF (2011) An insight into Mn(II) chemistry: a study of reaction kinetics under alkaline conditions. Int J Chem Res 2(4):34–37
12. Oriňáková R, Turonová A, Kladeková D, Gálová M, Smith RM (2006) Recent developments in the electrodeposition of nickel and some nickel-based alloys. J Appl Electrochem 36:957–972
13. Rudnik E, Wojnicki M, Włoch G (2012) Effect of gluconate addition on the electrodeposition of nickel from acidic baths. Surf Coat Technol 207:375–388
14. Chen K, Wilcox GD (2006) Tin-manganese alloy electrodeposits. J Electrochem Soc 153(9):C634–C640
15. Wu J, Jiang Y, Johson C, Liu X (2008) DC electrodeposition of Mn-Co alloys on stainless steels for SOFC interconnect application. J Power Sources 177:376–385
16. Gonsalves M, Pletcher D (1990) A study of the electrodeposition of manganese from aqueous chloride electrolytes. J Electroanal Chem 285:185–193
17. Diaz-Arista P, Trejo G (2006) Electrodeposition and characterization of manganese coatings obtained from an acidic chloride bath containing ammonium thiocyanate as an additive. Surf Coat Technol 201:3359–3367
18. Gong J, Zangari G (2002) Electrodeposition and characterization of manganese coatings. J Electrochem Soc 149(4):C209–C217
19. (1998) MINTEQA2/PRODEFA2, A geochemical assessment model for environmental systems: user manual supplement for version 4.0
20. Felmy AR, Mason MJ, Qafoku O (2003) Thermodynamic data development for modeling Sr/TRU separations: Sr-EDTA, Sr-HEDTA and Mn-gluconate complexation. Battelle Memorial Institute, Washington
21. Bodini ME, Sawyer DT (1976) Electrochemical and spectroscopic studies of Mn(II), Mn(III) and Mn(IV) gluconate complexes. Inorg Chem 15(7):1538–1543
22. Escandar GM, Peregrin JM, Sierra MG, Martino D et al (1996) Interaction of divalent metal ions with D-gluconic acid in the solid phase and aqueous solution. Polyhed 15(13):2251–2261
23. Pourbaix M (1966) Atlas of electrochemical equilibria in aqueous solutions. Pergamon, New York
24. Fleischmann M, Saraby-Reintjes A (1984) The simultaneous deposition of nickel and hydrogen on vitreous carbon. Electrochim Acta 29(1):69–75